Isospin Symmetry Breaking Disclosed in the Decay of Three-Proton Emitter 20Al

Isospin Symmetry Breaking Disclosed in the Decay of Three-Proton Emitter ^{20}Al

X.-D. Xu,[1,2,3,*] I. Mukha,[3,†] J. G. Li,[1,2,4] S. M. Wang,[5,6] L. Acosta,[7,8] M. Bajzek,[3,9,10] E. Casarejos,[11] D. Cortina-Gil,[12] J. M. Espino,[13] A. Fomichev,[14] H. Geissel,[3,9,‡] J. Gómez-Camacho,[13] L. V. Grigorenko,[14,15,16] O. Kiselev,[3] A. A. Korsheninnikov,[16] D. Kostyleva,[3] N. Kurz,[3] Yu. A. Litvinov,[3] I. Martel,[17] C. Nociforo,[3] M. Pfützner,[18,3] C. Rodríguez-Tajes,[19] C. Scheidenberger,[3,9,20] M. Stanoiu,[21] K. Sümmerer,[3] H. Weick,[3] P. J. Woods,[22] and M. V. Zhukov[23]

[1]*Institute of Modern Physics, Chinese Academy of Science, Lanzhou 730000, China*
[2]*School of Nuclear Science and Technology, University of Chinese Academy of Sciences, Beijing 100049, China*
[3]*GSI Helmholtzzentrum für Schwerionenforschung GmbH, 64291 Darmstadt, Germany*
[4]*Southern Center for Nuclear-Science Theory (SCNT), Institute of Modern Physics, Chinese Academy of Sciences, Huizhou 516000, China*
[5]*Key Laboratory of Nuclear Physics and Ion-beam Application (MOE), Institute of Modern Physics, Fudan University, Shanghai 200433, China*
[6]*Shanghai Research Center for Theoretical Nuclear Physics, NSFC and Fudan University, Shanghai 200438, China*
[7]*Instituto de Estructura de la Materia, CSIC, 28006 Madrid, Spain*
[8]*Instituto de Física, Universidad Nacional Autónoma de México, Apartado Postal 20-364, Mexico City 01000, Mexico*
[9]*II.Physikalisches Institut, Justus-Liebig-Universität, 35392 Gießen, Germany*
[10]*Faculty of Science, University of Zagreb, 10000 Zagreb, Croatia*
[11]*CINTECX, Universidade de Vigo, E-36310 Vigo, Spain*
[12]*Instituto de Física Corpuscular, CSIC - Universidad de Valencia, 46980, Paterna, Valencia, Spain*
[13]*Department of Atomic, Molecular and Nuclear Physics, University of Seville, 41012 Seville, Spain*
[14]*Flerov Laboratory of Nuclear Reactions, JINR, 141980 Dubna, Russia*
[15]*National Research Nuclear University "MEPhI", 115409 Moscow, Russia*
[16]*National Research Centre "Kurchatov Institute", Kurchatov square 1, 123182 Moscow, Russia*
[17]*University of Huelva, 21007 Huelva, Spain*
[18]*Faculty of Physics, University of Warsaw, 02-093 Warszawa, Poland*
[19]*Universidade de Santiago de Compostela, 15782 Santiago de Compostela, Spain*
[20]*Helmholtz Research Academy Hesse for FAIR (HFHF), GSI Helmholtz Center for Heavy Ion Research, Campus Gießen, 35392 Gießen, Germany*
[21]*IFIN-HH, Post Office Box MG-6, Bucharest, Romania*
[22]*University of Edinburgh, EH1 1HT Edinburgh, United Kingdom*
[23]*Department of Physics, Chalmers University of Technology, S-41296 Göteborg, Sweden*

(Received 24 December 2024; revised 20 April 2025; accepted 31 May 2025; published 10 July 2025)

The previously unknown nucleus ^{20}Al has been observed for the first time by detecting its in-flight decays. Tracking trajectories of all decay products with silicon microstrip detectors allowed for a conclusion that ^{20}Al is unbound with respect to three-proton ($3p$) emission. The $3p$-decay energy of the ^{20}Al ground state has been determined to be $1.93(^{+0.12}_{-0.10})$ MeV through a detailed study of angular correlations of its decay products, $^{17}\mathrm{Ne}+p+p+p$. This value is significantly smaller than the predictions inferred from the isospin symmetry by using the known neutron separation energy of its mirror nucleus ^{20}N, which indicates a possible isospin symmetry breaking in the mirror nuclei ^{20}Al and ^{20}N. This observed isospin symmetry breaking is supported by the calculations of the continuum embedded theoretical frameworks, describing the observed ^{20}Al ground state as a $1p$ s-wave state with a spin-parity of 1^-, which differs from the spin-parity (2^-) of the ^{20}N ground state. The ^{20}Al ground state decays by sequential $1p$-$2p$ emission via the intermediate ground state of ^{19}Mg, which is the first observed case of "daughter" $2p$ radioactivity following $1p$ decay of the parent state.

*Contact author: xiaodong.xu@impcas.ac.cn
†Contact author: I.Mukha@gsi.de
‡Deceased.

DOI: 10.1103/hkmy-yfdk

Nuclear structure beyond the proton drip line was addressed in various studies of the light- and intermediate-mass nuclei, e.g., a recent review in Ref. [1]. The current research status can be summarized as follows. (i) All known $1p$ and $2p$ emitters are located by 1–2 atomic mass units (*amu*) beyond the proton drip line. The $2p$ emitters exhibit three main decay mechanisms (direct, sequential, and democratic) and their transition modes [2]. (ii) The most exotic nuclei located in the very remote outskirts of the nuclear landscape become unbound with respect to new decay channels. Such exotic decay modes play an increasingly important role as the precursor's decay energy increases. The most remote isotopes are identified as far as 4 *amu* beyond the proton drip line and decay by emission of 3 or 4 protons. (iii) The studied $3p$ and $4p$ decays show sequential decay mechanisms such as $1p$-$2p$ and $2p$-$2p$ emissions, respectively. In particular, the measured $3p$-decay patterns for all known $3p$ emitters (i.e., ^{7}B [3], ^{17}Na [4], ^{31}K [5], and ^{13}F [6]) include $2p$ emission as part of a sequential $1p$-$2p$ decay mechanism. More multiproton decay modes are reported; e.g., $5p$ emission from ^{9}N [7], and even $6p$ emission is foreseen from yet unobserved ^{20}Si. (iv) A mirror symmetry emerged from the isobaric-spin formalism means that a pair of nuclei with the same mass number but with reversed numbers of protons and neutrons should have an identical set of states including their ground state (i.e., with the same total angular momentum J and parity π). Based on the isospin symmetry, theoretical predictions for proton-unbound isotopes using their neutron-rich mirror partners reveal that an area of 5–6 *amu* beyond the proton drip line may be expected [8].

In our present Letter, we continue the "excursion beyond the proton drip line" of Refs. [8–10] and focus on the previously unobserved $3p$-unbound isotope ^{20}Al using data obtained from a ^{20}Mg secondary beam [11]. Based on the analysis results, the isospin symmetry of the ^{20}Al–^{20}N mirror pair is examined.

The experiment was described in detail in Refs. [12,13]. The ^{20}Mg beam was produced by the fragmentation of a primary 591 *A*MeV ^{24}Mg beam at the SIS-FRS facility at GSI, Germany. The main objective of the experiment was study of $2p$ decays of ^{19}Mg nuclei in flight. A brief summary of the experimental setup and detector performance is given below. The FRS was operated with ion-optical settings in a separator-spectrometer mode, where the first half of the FRS was set for separation and focusing of the radioactive beams on a secondary target in the middle of the FRS, and the second half of the FRS was set for the detection of heavy-ion (HI) decay products. The secondary ^{20}Mg beam with an energy of 450 *A*MeV and an intensity of 400 ions s^{-1} bombarded a 2 g/cm^2 ^{9}Be secondary target located at the FRS middle focal plane; see details in Refs. [11,13]. The ^{19}Mg nuclei were produced via a neutron-knockout reaction with the ^{20}Mg projectiles. The decay products of unbound ^{19}Mg nuclei were tracked by a double-sided silicon microstrip detector (DSSD) array placed just downstream of the secondary target. Four large-area DSSDs [14] were employed to measure hit coordinates of the protons and the recoil heavy ions, resulting from the in-flight decays of the $2p$ precursors. The high-precision position measurement by DSSDs allowed for reconstruction of all fragment trajectories, enabling us to derive the decay vertex together with angular HI-p and HI-p-p correlations. Based on the trajectories of $^{17}\mathrm{Ne}+p+p$ measured in coincidence [13], several states including the ground state (g.s.) of ^{19}Mg were observed and spectroscopic information on these states was obtained using angular HI-p correlations as a function of their root-mean-square angle,

$$\rho_\theta = \sqrt{\theta^2_{p_1-^{17}\mathrm{Ne}} + \theta^2_{p_2-^{17}\mathrm{Ne}}}. \quad (1)$$

Several by-product results were obtained similarly from the data recorded during the experiment. In particular, the $3p$-unbound nucleus ^{20}Al was produced in a charge-exchange reaction. This mechanism has a smaller cross section than knockout reactions, leading to the ^{20}Al data having fewer statistics than the ^{19}Mg data [13]. Nevertheless, they may provide the first hints on nuclear structure of the previously unobserved ^{20}Al. The ^{20}Al spectrum was derived from the trajectories and angular correlations of all decay products $^{17}\mathrm{Ne}+p_1+p_2+p_3$, which were measured in four-fold coincidence. Given that the ^{19}Mg g.s. was identified by a careful analysis of the $^{17}\mathrm{Ne}+2p$ correlations in previous studies [11,13], this could serve as a basis for analyzing the $^{17}\mathrm{Ne}+3p$ correlations to search for the ^{20}Al g.s. The detector calibration coefficients were taken from the analysis reported in Refs. [12,13], and the same data analysis procedure applied to $3p$ decays of ^{31}K [5] was employed for ^{20}Al.

The measured trajectories of $^{17}\mathrm{Ne}+3p$ coincident events were used for deriving relative angles between each proton and ^{17}Ne. Then a kinematic variable ρ_3 was introduced for $3p$ decays in analogy with $2p$ decays [see Eq. (1)] and its expression is as follows:

$$\rho_3 = \sqrt{\theta^2_{p_1-^{17}\mathrm{Ne}} + \theta^2_{p_2-^{17}\mathrm{Ne}} + \theta^2_{p_3-^{17}\mathrm{Ne}}}. \quad (2)$$

The emitted protons share the $3p$-decay energy; thus, ρ_3 is very useful for illustration of the states in the $3p$-decay precursor, as it was shown in the ^{31}K spectroscopy [5].

The ρ_3 distribution derived from the measured $^{17}\mathrm{Ne}+3p$ correlations following ^{20}Al decays is shown in Fig. 1(a). The corresponding total $3p$-decay energies E_T

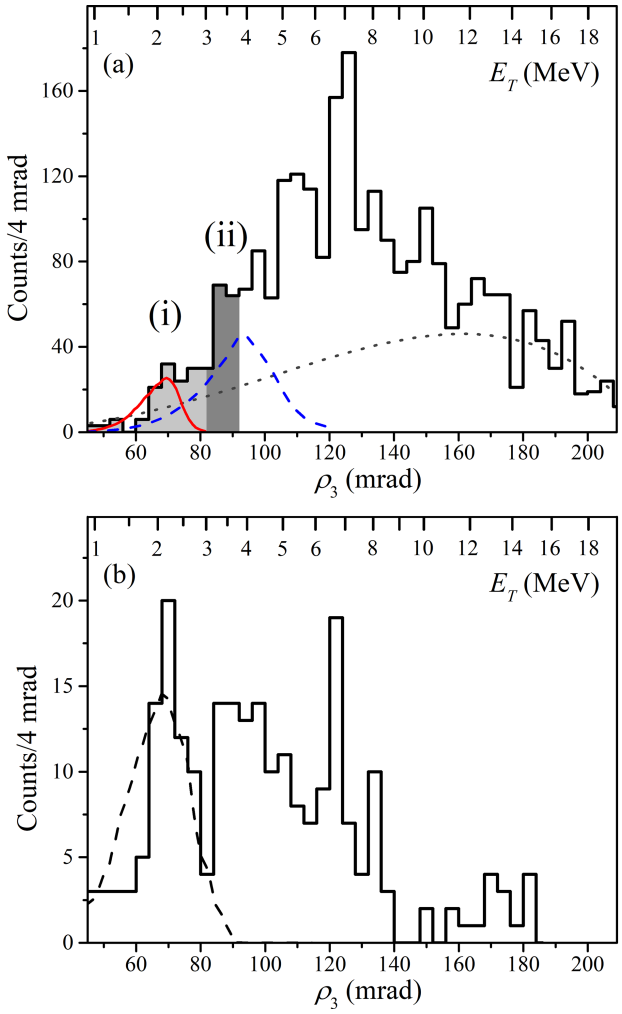

FIG. 1. (a) Three-proton angular correlations ρ_3 derived from the measured trajectories of all decay products, $^{17}\mathrm{Ne}+3p$ (histogram), which reflect the total $3p$-decay energy E_T of the ^{20}Al states shown in the upper axis. The shaded areas indicate the ρ_3 gates employed for the selection of peak (i) and peak (ii), where populations of the two lowest states in ^{20}Al are expected. The illustrative simulations of the $3p$ decays of ^{20}Al with the assumed E_T of 2.0 and 3.6 MeV are shown by the solid and dashed curves, respectively. The dotted curve shows a four-body phase volume simulation for a direct reaction with an exit channel $^{17}\mathrm{Ne}+3p$ in the absence of any resonance in ^{20}Al. (b) Similar distribution as in (a) but gated in addition by small angles $20 < \theta_{p-^{17}\mathrm{Ne}} < 40$ mrad, which are typical for the ^{19}Mg g.s. decay (see the area under dash-dotted curve in Fig. 2). The dashed curve shows simulations of the $3p$ decay of ^{20}Al with $E_T = 2.0$ MeV.

can be estimated from the upper axis. One can see that the low-energy part cannot be described by a four-body phase volume simulation for a direct reaction with an exit channel $^{17}\mathrm{Ne}+3p$ in the absence of any resonance in ^{20}Al. The four-body phase volume is proportional to an $E_T^{7/2}$ factor [15] multiplied to the detection efficiency of events $^{17}\mathrm{Ne}+3p$. It is normalized to the measured intensity at small and large ρ_3 values, ≤ 60 and ≥ 160 mrad, respectively. Due to this normalization, the four-body phase-volume component represents an upper-limit estimate of the possible contribution of the nonresonant branch in the measured correlations. The data significantly exceed the estimated nonresonant contribution, and therefore low energy ^{20}Al resonance contributions are required to describe these measured angular correlations. The proton separation energy (S_p) of ^{20}Al was predicted by the systematics proposed for the mass differences of mirror nuclei [16,17]. The estimated E_T values for the ^{20}Al g.s. are 3.4–3.6 MeV, which reduce the inspected angular correlations to the range below 100 mrad [see Fig. 1(a)]. There are a few bumps in the ρ_3 spectrum above 100 mrad, e.g., located at E_T of ~5 and ~7 MeV, which may correspond to higher excited states in ^{20}Al. In this Letter, we focus on searching for the lowest states, particularly the g.s. of ^{20}Al.

With the predicted E_T values, ^{20}Al g.s. should be open to a sequential $1p$-$2p$ decay mechanism via the intermediate g.s. of ^{19}Mg. The known decay pattern of the ^{19}Mg g.s. shows the $\theta_{p-^{17}\mathrm{Ne}}$ correlations ranging from 20 to 40 mrad [13]. Thus the measured ρ_3 correlations may be exclusively inspected by implementing a selective $\theta_{p-^{17}\mathrm{Ne}}$ gate. We produced the exclusive ρ_3 distribution by applying the gate in the $\theta_{p-^{17}\mathrm{Ne}}$ range of 20–40 mrad, which is typical for the ^{19}Mg g.s. decay. As a result, the low-energy states in ^{20}Al decaying via the ^{19}Mg g.s. should be conserved in comparison to higher-energy states, which are open to several decay channels in larger $\theta_{p-^{17}\mathrm{Ne}}$ ranges and therefore should be suppressed. Figure 1(b) shows the gated ρ_3 distribution where there are two prominent peaks at E_T of 2.0 and 3.6 MeV, which suggest two low-lying states in ^{20}Al. For the purposes of illustration, two possible states in ^{20}Al assumed at E_T of 2.0 and 3.6 MeV are shown in Fig. 1(a). Their contributions are obtained by the GEANT simulations of the detector response to the decays of interest and the data analysis applied to ρ_3 angular correlations, see descriptions in the Appendix A. The simulated peak regions are labeled as (i) and (ii).

In order to study the low-lying states in ^{20}Al and establish their decay schemes quantitatively, the events located around the ρ_3 regions (i) and (ii) in Fig. 1(a) were selected, and the respective angular $\theta_{p-^{17}\mathrm{Ne}}$ correlations were examined. Figure 2 displays the $\theta_{p-^{17}\mathrm{Ne}}$ distribution by imposing the ρ_3 gate (i). The lowest-energy bump (i) around 2 MeV may correspond to the ^{20}Al g.s., which decays by emission of a proton into an intermediate state, ^{19}Mg ground state. The $2p$-decay energy (Q_{2p}) of ^{19}Mg g.s. has been measured to be 0.76(6) MeV [13,18], and a recent experiment utilizing the invariant mass method has yielded a very similar Q_{2p} value [19]. The corresponding $\theta_{p-^{17}\mathrm{Ne}}$ correlations in Fig. 2 should consist of two contributions. The first-emitted proton into the intermediate state in ^{19}Mg is

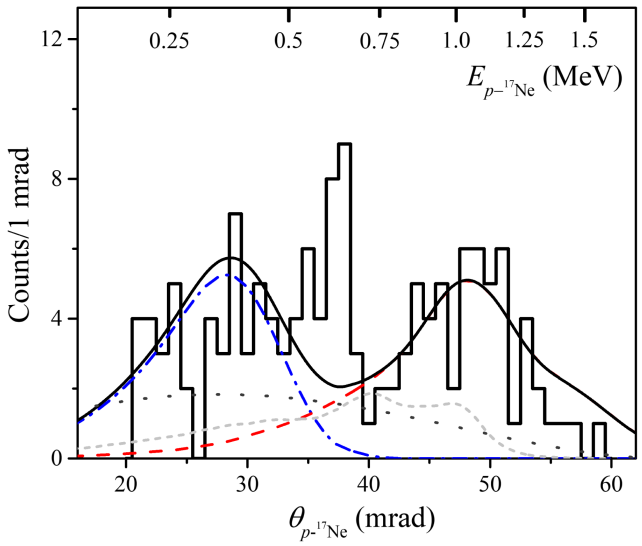

FIG. 2. Angular $\theta_{p-^{17}\mathrm{Ne}}$ correlations (histogram) derived from the measured $^{17}\mathrm{Ne}+3p$ coincidences by using the selection gate (i) in the $45<\rho_3<82$ mrad range shown in Fig. 1(a). The corresponding $1p$-decay energies $E_{p-^{17}\mathrm{Ne}}$ are given by the upper axis. The simulated contribution from an initial $1p$ decay of ^{20}Al into the ^{19}Mg g.s. with the Q_{1p} of $1.17(^{+0.10}_{-0.08})$ MeV is shown by the dashed curve. The contribution of a subsequent $2p$ decay of ^{19}Mg g.s. with the known decay energy of 0.76(6) MeV [13] is shown by the dash-dotted curve. The solid curve is their sum corresponding to $E_T=1.93(^{+0.12}_{-0.10})$ MeV. The dotted curve is the upper-limit estimate of the nonresonant contribution by using four-body phase-volume simulations. The short-dashed curve represents the estimated contribution from the tail of the neighboring ^{20}Al excited state, i.e., peak (ii) shown in Fig. 1(a).

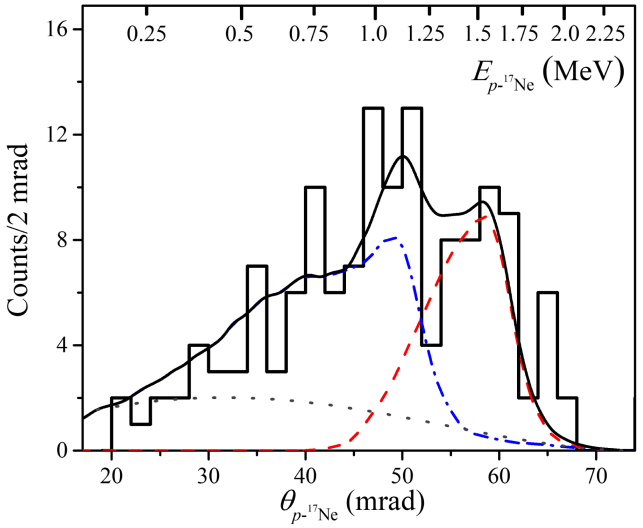

FIG. 3. Angular $\theta_{p-^{17}\mathrm{Ne}}$ correlations (histogram) derived from the measured $^{17}\mathrm{Ne}+3p$ coincidences by using the selection gate (ii) in the $82<\rho_3<92$ mrad range shown in Fig. 1(a). The corresponding $1p$-decay energies $E_{p-^{17}\mathrm{Ne}}$ are given by the upper axis. The simulated contribution from the primary $1p$ decay of $^{20}\mathrm{Al}^*$ into the first excited state in $^{19}\mathrm{Mg}^*$ [at $Q_{2p}=2.1(2)$ MeV] with the Q_{1p} of 1.50(10) MeV is shown by the dashed curve. The contribution of secondary-emitted protons from the $^{19}\mathrm{Mg}^*$ into the ^{17}Ne g.s. measured in Ref. [13] is shown by the dash-dotted curve. The solid curve shows their sum. The dotted curve represents the upper-limit estimate of the nonresonant contribution by using four-body phase-volume simulations.

expected to cause a peak in the observed $\theta_{p-^{17}\mathrm{Ne}}$ correlations. The second component should have the same shape as the known relatively broad $\theta_{p-^{17}\mathrm{Ne}}$ distribution from the ^{19}Mg g.s. $2p$-decay [13,18], which is centered around $E_{p-^{17}\mathrm{Ne}}\simeq 0.38$ MeV (because two identical protons share the total decay energy of 0.76 MeV). We have evaluated the data distribution in Fig. 2 by summing the two respective components: 1) the simulation of the detector response to the $1p$-emission of ^{20}Al (the simulation procedure is described in Refs. [12,13]); 2) the known detector response to the $2p$ decay of ^{19}Mg g.s. (see Refs. [13,18]). One may see that the small-angle region of the $\theta_{p-^{17}\mathrm{Ne}}$ distribution is described by the $2p$ decay of ^{19}Mg g.s. (the dash-dotted curve reflects the known Q_{2p} value of 0.76 MeV), while the large-angle correlations can be described by the $1p$ emission of ^{20}Al into ^{19}Mg g.s. (dashed curve) with the estimated $1p$-decay energy (Q_{1p}) of $1.17(^{+0.10}_{-0.08})$ MeV, leading to the total $3p$-decay energy $E_T=1.93(^{+0.12}_{-0.10})$ MeV. More details on deriving E_T values together with an estimation of the half-life of ^{20}Al can be found in the Appendixes A and C.

The angular $\theta_{p-^{17}\mathrm{Ne}}$ correlations obtained by selection using the ρ_3 gate (ii) in Fig. 1(a) are shown in Fig. 3. Such a selection is aimed at an excited state in ^{20}Al located around $E_T\simeq 3.6$ MeV. One may see two bumps dominating the selected distribution at the angles of ~50 and ~58 mrad. These bumps are attributed to the sequentially emitted protons from $^{20}\mathrm{Al}^*$ via an intermediate state in $^{19}\mathrm{Mg}^*$ [$Q_{2p}=2.1(2)$ MeV] and its subsequent $2p$ decay via one ^{18}Na state [13]. The angular correlations from the $2p$ decay of the intermediate 2.1-MeV state in ^{19}Mg have been measured and described in Ref. [13]. The respective simulation taken from Fig. 4(b) of Ref. [13] is shown in Fig. 3 (dash-dotted curve normalized to the data). The dash-dotted curve is double-humped since it represents sequential $^{19}\mathrm{Mg}^*\rightarrow{}^{18}\mathrm{Ne}+p\rightarrow{}^{17}\mathrm{Ne}+2p$ decays as explained in Fig. 4(b) of Ref. [13]. The contribution of the first-emitted proton is shown by the dashed curve. The sum of these two contributions matches the data with probability of 0.993 when the energy of the first-emitted proton is 1.50(10) MeV. The $1p$-decay energy and its uncertainties are derived similarly to those of the ^{20}Al g.s. Taking the energy of the secondary- and tertiary-emitted protons $Q_{2p}=2.1(2)$ MeV into account, the total $3p$-decay energy is 3.60(22) MeV.

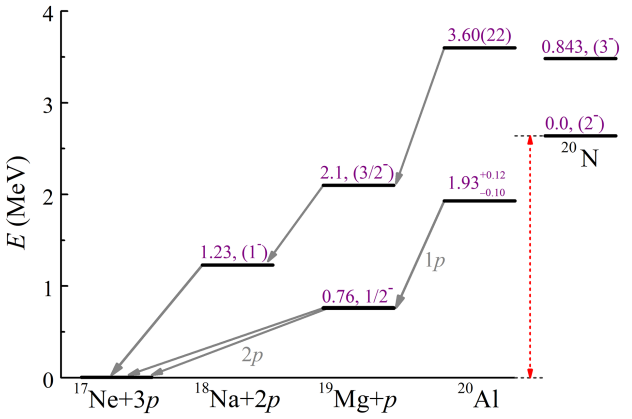

FIG. 4. Proposed decay scheme of the two lowest states in ^{20}Al with tentatively assigned decay channels via the known ^{19}Mg and ^{18}Na ground states [13], whose energies are given relative to the $3p$, $2p$ and $1p$ thresholds, respectively. On the right-hand side, the two lowest levels of ^{20}N are shown. They are shifted by the MED expected for the $s_{1/2}$ $1p$ configuration in the ^{20}N–^{20}Al pair, which corresponds to the closest prediction $S_{3p}(^{20}\mathrm{Al}) = -2.64$ MeV; see the vertical dotted arrow.

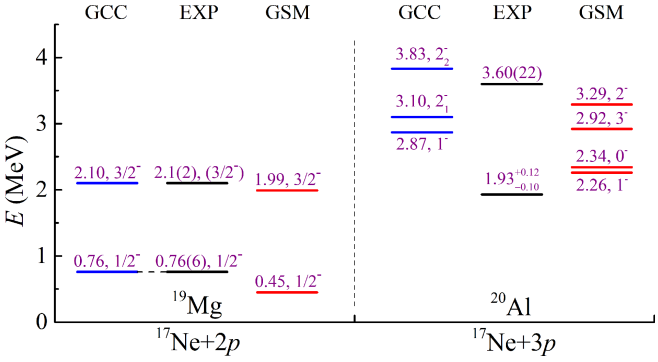

FIG. 5. The experimental energies of the lowest states in ^{20}Al and those of ^{19}Mg compared to the two model predictions. The energy values are provided with respect to the $3p$ and $2p$ thresholds, respectively.

The assigned energies of two low-lying states in ^{20}Al and their decay scheme are displayed in Fig. 4. Based on the decay energy of ^{20}Al g.s. and the masses of $^{17}\mathrm{Ne} + 3p$, the mass excess of ^{20}Al has been determined to be 40.30(12) MeV. The ^{20}Al mass predicted by the improved Kelson-Garvey mass relations [16,17] [the evaluated $3p$-separation energy (S_{3p}) value is $-(3.4\text{–}3.6)$ MeV] shows a significant discrepancy compared to the data. Such a difference may be explained by the effect of Thomas-Ehrmann shift (TES) [20,21] which is often observed in $1p$-unbound nuclei. Indeed, as the ^{20}Al g.s. decays via the relatively long-lived ^{19}Mg g.s., one may use the empirical S_p systematics derived from the known $1p$-emitting states in light nuclei. It is based on a parametrization of the mirror energy difference (MED) [22]. The definition of MED is MED = S_n(neutron-rich nucleus) − S_p(its proton-righ mirror), and the parametrization is MED = $(Z/A^{1/3})$MED′, where the MED′ value does not depend on the proton number Z and mass number A [22]. We evaluated the S_p value and then derived the S_{3p} value for the ^{20}Al g.s. by using the known S_n value of its mirror partner $^{20}\mathrm{N}_{g.s.}(2^-)$ and the corresponding MED value taken from the parametrization [22]. If the ^{20}Al g.s. is an s-wave state, the predicted $S_{3p}(^{20}\mathrm{Al})$ is -2.64 MeV. This indicates that the $3p$-decay energy prediction for ^{20}Al g.s. is 0.71 MeV higher than the data (see Fig. 4). If the ^{20}Al g.s. is a $d_{5/2}$ state, the parametrization results in $S_{3p}(^{20}\mathrm{Al}) = -3.42$ MeV, demonstrating that the predicted $3p$-decay energy is even higher than the data. Thus we conclude that the TES may partly explain the observed lowering of $3p$-unbound g.s. of ^{20}Al in comparison with its bound isospin mirror ^{20}N, though the observed lowering effect is significantly larger. Furthermore, we investigated the systematics of odd-even staggering energies for nitrogen isotopes and their mirror nuclei, including the ^{20}N-^{20}Al mirror pair, as presented in the Appendix B.

We calculated low-lying states of ^{20}Al and its $1p$-decay daughter nucleus ^{19}Mg by employing the Gamow Shell Model (GSM) [23–25] and Gamow coupled-channel (GCC) model [26–28]. A brief description of the models and corresponding calculation details can be found in the Appendixes D and E. Figure 5 compares the model predictions with the data. The GSM provides a reasonable description of both ^{19}Mg $1/2^-$ g.s. and $(3/2^-)$ excited state, in particular, the energy of $(3/2^-)$ excited state is well reproduced within the experimental uncertainty. In the GCC model calculations, the energies of $1/2^-$ and $(3/2^-)$ states in ^{19}Mg were employed to adjust the free parameters. Its predictions for ^{20}Al indicate that the g.s. has a spin-parity of 1^- and is located 2.87 MeV above the $3p$ threshold. The GSM also predicts $J^\pi = 1^-$ for the ^{20}Al g.s., which is positioned at 2.26 MeV above the $3p$ threshold. These results demonstrate that the ^{20}Al g.s. has a dominant $s_{1/2}$ $1p$-configuration, which differs from its mirror ^{20}N g.s. with the $J^\pi = (2^-)$. In addition to the energy shift of the ^{20}Al g.s. relative to the ^{20}N g.s., the spin-parity difference provides further evidence of isospin symmetry breaking in the ^{20}Al–^{20}N mirror pair. Regarding the excited states of ^{20}Al, several low-energy levels are predicted by GSM. The level predicted to be closest to the observed 3.6 MeV state is situated at 3.29 MeV above the $3p$ threshold and has the $J^\pi = 2^-$. The GCC model predicts two excited states with a spin-parity of 2^-, and the one closest to the 3.6 MeV state in energy is located at 3.83 MeV above the $3p$ threshold. Therefore, $J^\pi = (2^-)$ may be tentatively assigned to the observed 3.6 MeV state.

The discussed difference in the observed and predicted energies of the ^{20}Al g.s. is not unique. Similar lowering of g.s. energy has been observed in another $3p$-emitter ^{31}K

with a $(d_{5/2})^3$ configuration, which may indicate additional binding stemming from a nuclear structure effect that requires further investigations, such as employing the three-body forces [29–31]. The data on other $3p$-emitters, e.g., the unidentified-yet g.s. of ^{13}F or ^{17}Na with a presumed $(sd)^3$ configuration, are also needed.

The observation of the $3p$-unbound ^{20}Al g.s. leads to the prediction that its neighboring isotope ^{21}Si is a $4p$ emitter. Taking into account that the predicted $S_{2p}(^{21}\mathrm{Si}) = -3.7$ MeV [32], one may derive its $S_p = -2.53$ MeV and therefore expect a triple sequential $1p$-$1p$-$2p$ emission from the unobserved-yet g.s. of ^{21}Si.

In conclusion, the first spectroscopy of the previously unknown isotope ^{20}Al which decays by $3p$ emission, has revealed that the decay energy of ^{20}Al ground state is significantly smaller than the predictions inferred from the isospin symmetry. The mass excess of the ^{20}Al g.s. has been derived from the measured S_{3p} value to be 40.30(12) MeV, which is a challenging test for predictions by nuclear mass models. The observed effect of increased Thomas-Ehrman shift of the $3p$-unbound ^{20}Al g.s. can be explained by both GSM and GCC model calculations, where the s-wave component of valence protons is dominant, leading to the prediction of $J^\pi = 1^-$. This indicates a violation of the isospin symmetry in comparison with the (2^-) g.s. of mirror partner ^{20}N. The observed effect of lowering of the ^{20}Al g.s. is similar to that detected in another $3p$-emitter ^{31}K, which indicates a possible phenomenon of nuclear-structure preservation far beyond the proton drip line, thereby calling for further systematic investigations. If the effect of nuclear-structure preservation is confirmed, the region of existence of proton(s) resonances in nuclear chart would be broader compared to the previous estimates based on the isospin symmetry, i.e., the number of unknown isotopes is larger, and the transition region to chaotic nuclear systems is located further from the proton drip line in comparison with the previous predictions [8].

Acknowledgments—This Letter was partially supported by the Helmholtz International Center for FAIR (HIC for FAIR); the Chinese Academy of Sciences President's International Fellowship Initiative (Grant No. 2024PVA0005); the National Key Research and Development Program (MOST 2022YFA1602303 and MOST 2023YFA1606404), the National Natural Science Foundation of China (Grants No. 12347106, No. 12147101, and No. 12205340); the Gansu Natural Science Foundation under Grant No. 22JR5RA123; the European Union's Horizon Europe Research and Innovation program under Grant Agreement No. 101057511 (EURO-LABS); the Helmholtz Association (Grant IK-RU-002); the Russian Science Foundation (Grant No. 22-12-00054); the Polish National Science Center (Contract No. 2019/33/B/ST2/02908); the Helmholtz-CAS Joint Research Group (Grant HCJRG-108); the Ministry of Education & Science, Spain (Contract No. FPA2016-77689-C2-1-R); the Ministry of Economy, Spain (Grant FPA2015-69640-C2-2-P); the Hessian Ministry for Science and Art (HMWK) through the LOEWE funding scheme; the Justus-Liebig-Universität Giessen (JLU) and the GSI under the JLU-GSI strategic Helmholtz partnership agreement; and DGAPA-PAPIIT IG101423. This research was supported in part in the framework of scientific program of the Russian National Center for Physics and Mathematics, topic number 6 "Nuclear and radiation physics" (2023–2025 stage). This work was carried out in the framework of the Super-FRS Experiment Collaboration.

Data availability—The data that support the findings of this Letter are not publicly available. The data are available from the authors upon reasonable request.

[1] M. Pfützner, I. Mukha, and S. M. Wang, Prog. Part. Nucl. Phys. **132**, 104050 (2023).
[2] T. Golubkova, X.-D. Xu, L. Grigorenko, I. Mukha, C. Scheidenberger, and M. Zhukov, Phys. Lett. B **762**, 263 (2016).
[3] R. J. Charity, J. M. Elson, J. Manfredi, R. Shane, L. G. Sobotka, B. A. Brown, Z. Chajecki, D. Coupland, H. Iwasaki, M. Kilburn *et al.*, Phys. Rev. C **84**, 014320 (2011).
[4] K. W. Brown, R. J. Charity, J. M. Elson, W. Reviol, L. G. Sobotka, W. W. Buhro, Z. Chajecki, W. G. Lynch, J. Manfredi, R. Shane *et al.*, Phys. Rev. C **95**, 044326 (2017).
[5] D. Kostyleva, I. Mukha, L. Acosta, E. Casarejos, V. Chudoba, A. A. Ciemny, W. Dominik, J. A. Dueñas, V. Dunin, J. M. Espino *et al.*, Phys. Rev. Lett. **123**, 092502 (2019).
[6] R. J. Charity, T. B. Webb, J. M. Elson, D. E. M. Hoff, C. D. Pruitt, L. G. Sobotka, K. W. Brown, G. Cerizza, J. Estee, W. G. Lynch *et al.*, Phys. Rev. Lett. **126**, 132501 (2021).
[7] R. J. Charity, J. Wylie, S. M. Wang, T. B. Webb, K. W. Brown, G. Cerizza, Z. Chajecki, J. M. Elson, J. Estee, D. E. M. Hoff *et al.*, Phys. Rev. Lett. **131**, 172501 (2023).
[8] L. V. Grigorenko, I. Mukha, D. Kostyleva, C. Scheidenberger, L. Acosta, E. Casarejos, V. Chudoba, A. A. Ciemny, W. Dominik, J. A. Dueñas *et al.*, Phys. Rev. C **98**, 064309 (2018).
[9] I. Mukha, L. V. Grigorenko, D. Kostyleva, L. Acosta, E. Casarejos, A. A. Ciemny, W. Dominik, J. A. Dueñas, V. Dunin, J. M. Espino *et al.*, Phys. Rev. C **98**, 064308 (2018).
[10] D. Kostyleva, X.-D. Xu, I. Mukha, L. Acosta, M. Bajzek, E. Casarejos, A. A. Ciemny, D. Cortina-Gil, W. Dominik, J. A. Dueñas *et al.*, Phys. Rev. C **110**, L031301 (2024).
[11] I. Mukha, K. Sümmerer, L. Acosta, M. A. G. Alvarez, E. Casarejos, A. Chatillon, D. Cortina-Gil, J. Espino, A. Fomichev, J. E. Garcia-Ramos *et al.*, Phys. Rev. Lett. **99**, 182501 (2007).
[12] I. Mukha, K. Sümmerer, L. Acosta, M. A. G. Alvarez, E. Casarejos, A. Chatillon, D. Cortina-Gil, I. A. Egorova, J. M. Espino, A. Fomichev *et al.*, Phys. Rev. C **82**, 054315 (2010).
[13] I. Mukha, L. Grigorenko, L. Acosta, M. A. G. Alvarez, E. Casarejos, A. Chatillon, D. Cortina-Gil, J. M. Espino,

A. Fomichev, J. E. García-Ramos *et al.*, Phys. Rev. C **85**, 044325 (2012).
[14] M. Stanoiu, K. Sümmerer, I. Mukha, A. Chatillon, E. C. Gil, M. Heil, J. Hoffman, O. Kiselev, N. Kurz, and W. Ott (S271 Collaboration), Nucl. Instrum. Methods Phys. Res., Sect. B **266**, 4625 (2008).
[15] I. A. Muzalevskii, N. B. Shulgina, A. A. Bezbakh, V. Chudoba, S. A. Krupko, S. G. Belogurov, D. Biare, I. A. Egorova, A. S. Fomichev, E. M. Gazeeva *et al.*, Phys. Rev. C **111**, 014612 (2025).
[16] J. Tian, N. Wang, C. Li, and J. Li, Phys. Rev. C **87**, 014313 (2013).
[17] Y. Y. Zong, C. Ma, M. Q. Lin, and Y. M. Zhao, Phys. Rev. C **105**, 034321 (2022).
[18] X.-D. Xu, I. Mukha, L. V. Grigorenko, C. Scheidenberger, L. Acosta, E. Casarejos, V. Chudoba, A. A. Ciemny, W. Dominik, J. Duénas-Díaz *et al.*, Phys. Rev. C **97**, 034305 (2018).
[19] L. Ni, Y. Jin, Z. H. Li, K. W. Brown, C. X. Yuan, H. Hua, C. Y. Niu, A. K. Anthony, J. Barney, R. J. Charity *et al.*, Phys. Rev. C **110**, L061301 (2024).
[20] R. G. Thomas, Phys. Rev. **88**, 1109 (1952).
[21] J. B. Ehrman, Phys. Rev. **81**, 412 (1951).
[22] H. T. Fortune, Phys. Rev. C **97**, 034301 (2018).
[23] N. Michel, W. Nazarewicz, M. Płoszajczak, and K. Bennaceur, Phys. Rev. Lett. **89**, 042502 (2002).
[24] N. Michel, W. Nazarewicz, M. Płoszajczak, and T. Vertse, J. Phys. G **36**, 013101 (2009).
[25] J. G. Li, Y. Z. Ma, N. Michel, B. S. Hu, Z. H. Sun, W. Zuo, and F. R. Xu, Physics **3**, 977 (2021).
[26] S. M. Wang, N. Michel, W. Nazarewicz, and F. R. Xu, Phys. Rev. C **96**, 044307 (2017).
[27] S. M. Wang and W. Nazarewicz, Phys. Rev. Lett. **126**, 142501 (2021).
[28] S. M. Wang, W. Nazarewicz, R. J. Charity, and L. G. Sobotka, J. Phys. G **49**, 10LT02 (2022).
[29] J. D. Holt, J. Menéndez, and A. Schwenk, Phys. Rev. Lett. **110**, 022502 (2013).
[30] A. T. Gallant, J. C. Bale, T. Brunner, U. Chowdhury, S. Ettenauer, A. Lennarz, D. Robertson, V. V. Simon, A. Chaudhuri, J. D. Holt *et al.*, Phys. Rev. Lett. **109**, 032506 (2012).
[31] M. Wang, Y. H. Zhang, X. Zhou, X. H. Zhou, H. S. Xu, M. L. Liu, J. G. Li, Y. F. Niu, W. J. Huang, Q. Yuan *et al.*, Phys. Rev. Lett. **130**, 192501 (2023).
[32] H. T. Fortune, Phys. Rev. C **96**, 034304 (2017).
[33] S. Agostinelli, J. Allison, K. Amako, J. Apostolakis, H. Araujo, P. Arce, M. Asai, D. Axen, S. Banerjee, G. Barrand *et al.*, Nucl. Instrum. Methods Phys. Res., Sect. A **506**, 250 (2003).
[34] W. T. Eadie *et al.*, *Statistical Methods in Experimental Physics* (North-Holland, Amsterdam, 1971).
[35] Y. Yu, Y. M. Xing, Y. H. Zhang, M. Wang, X. H. Zhou, J. G. Li, H. H. Li, Q. Yuan, Y. F. Niu, Y. N. Huang *et al.*, Phys. Rev. Lett. **133**, 222501 (2024).
[36] J. W. Zhao, B.-H. Sun, I. Tanihata, J. Y. Xu, K. Y. Zhang, A. Prochazka, L. H. Zhu, S. Terashima, J. Meng, L. C. He *et al.*, Phys. Lett. B **858**, 139082 (2024).
[37] I. Mukha, L. V. Grigorenko, X. Xu, L. Acosta, E. Casarejos, A. A. Ciemny, W. Dominik, J. Duénas-Díaz, V. Dunin, J. M. Espino *et al.*, Phys. Rev. Lett. **115**, 202501 (2015).
[38] T. Berggren, Nucl. Phys. **A109**, 265 (1968).
[39] R. Id Betan, R. J. Liotta, N. Sandulescu, and T. Vertse, Phys. Rev. Lett. **89**, 042501 (2002).
[40] N. Michel and M. Płoszajczak, *Gamow Shell Model, The Unified Theory of Nuclear Structure and Reactions*, Lecture Notes in Physics Vol. 983 (Springer, Berlin, 2021).
[41] N. Michel, J. G. Li, L. H. Ru, and W. Zuo, Phys. Rev. C **106**, L011301 (2022).
[42] N. Michel, J. G. Li, F. R. Xu, and W. Zuo, Phys. Rev. C **103**, 044319 (2021).
[43] R. Machleidt and D. Entem, Phys. Rep. **503**, 1 (2011).
[44] E. Epelbaum, H.-W. Hammer, and Ulf-G. Meißner, Rev. Mod. Phys. **81**, 1773 (2009).
[45] Y. Jin, C. Y. Niu, K. W. Brown, Z. H. Li, H. Hua, A. K. Anthony, J. Barney, R. J. Charity, J. Crosby, D. Dell'Aquila *et al.*, Phys. Rev. Lett. **127**, 262502 (2021).
[46] J. G. Li, N. Michel, W. Zuo, and F. R. Xu, Phys. Rev. C **103**, 034305 (2021).
[47] J.-M. Sparenberg and D. Baye, Phys. Rev. Lett. **79**, 3802 (1997).
[48] S. M. Wang and W. Nazarewicz, Phys. Rev. Lett. **120**, 212502 (2018).
[49] D. R. Thompson, M. Lemere, and Y. C. Tang, Nucl. Phys. **A286**, 53 (1977).
[50] S. Cwiok, J. Dudek, W. Nazarewicz, J. Skalski, and T. Werner, Comput. Phys. Commun. **46**, 379 (1987).
[51] S. Saito, Suppl. Prog. Theor. Phys. **62**, 11 (1977).

End Matter

Appendix A: Derivation of the ^{20}Al *decay energies*—To determine the $3p$-decay energies of ^{20}Al states corresponding to the $\theta_{p-^{17}\mathrm{Ne}}$ angular correlations in Fig. 2, we performed Monte Carlo simulations of the detector response to the sequential $1p$-$2p$ decays of ^{20}Al states via intermediate ^{19}Mg by using the GEANT software [33], which was described in detail in Refs. [12,13]. Several simulations of ^{17}Ne-p angular correlations were performed. Each simulation contained two components: one component with a varied decay energy of $1p$ decay $^{20}\mathrm{Al} \rightarrow {}^{19}\mathrm{Mg}$ and the other component with a fixed $2p$-decay energy of ^{19}Mg g.s. ($Q_{2p} = 0.76$ MeV). The intrinsic widths of ^{20}Al states were assumed to be very small, i.e., 1 keV. Then every simulated spectrum was compared with the data by using the standard Kolmogorov test, which computes the probability that the simulated spectrum matches the respective experimental pattern [34]. According to the Kolmogorov test, two compared histograms are statistical variations of the same distribution if the Kolmogorov-test probability is larger than 0.5. The Q_{1p} values were derived from the distributions of the calculated probabilities with the

corresponding uncertainty. Consequently, the Q_{1p} value was determined to be $1.17^{+0.10}_{-0.08}$ MeV, which corresponds to descriptions of the data in Fig. 2 with the highest probability of 0.821. Regarding the impact of potential background, we evaluated the contributions of the nonresonant reaction (dotted curve in Fig. 2) and the tail of neighboring 3.6-MeV excited state of ^{20}Al (short-dashed curve in Fig. 2) quantitatively by including them as small admixtures in the simulation and comparing with data using the Kolmogorov test. The results demonstrate that the background can be neglected.

The $\theta_{p-^{17}\mathrm{Ne}}$ angular distribution in Fig. 2 has two irregular bins around 38 mrad (the corresponding $E_p \simeq 0.65$ MeV). Their sum intensity is estimated to be comparable with the $\sim 3\sigma$ statistical deviation of the contribution of the previously assumed $3p$-decay branch at the 38 mrad angle. Given the fact that the events of this "peak" are within the ρ_3 gate (i), this peak likely indicates another minor $3p$-decay channel with the total decay energy $E_T = 1.93$ MeV. However, it seems there are no states known (and/or predicted) in the intermediate ^{19}Mg and ^{18}Na nuclei which could match these E_T and E_p values. The origin of the peak around 38 mrad is unclear. Here we propose a tentative explanation for these events. A minor branch of $3p$ decay of the $^{20}\mathrm{Al}^*(E_T = 3.6\ \mathrm{MeV})$ state may proceed via three sequential proton emissions $^{20}\mathrm{Al}^* \rightarrow p + {}^{19}\mathrm{Mg}^*(Q_{2p} = 2.9\ \mathrm{MeV}) \rightarrow 2p + {}^{18}\mathrm{Na}^* \rightarrow 3p + {}^{17}\mathrm{Ne}^*(E^* = 1.288\ \mathrm{MeV})$, where intermediate state(s) in ^{18}Na are unresolved. Under this scenario, only the first emitted proton produced from $^{20}\mathrm{Al}^*$ to $^{19}\mathrm{Mg}^*$ was detected and the decay energy corresponds to the observed $\sim$0.65 MeV peak in Fig. 2 if $E_T = 3.55$ MeV. However, contributions of other emitted protons are unresolved. The 1.288 MeV state of ^{17}Ne de-excites by emitting a γ ray, which is undetected in our experiment. This speculative interpretation for the "peak" around 38 mrad is based solely on the decay energy matching. Future investigations with improved statistics and better resolution are required to elucidate its underlying mechanism.

Appendix B: Systematics of odd-even staggering energies—Comparisons of masses (e.g., Ref. [35]) or radii (e.g., Ref. [36]) of mirror nuclei are often employed to examine the isospin symmetry. Based on the obtained mass of ^{20}Al, we can study the systematics of odd-even staggering (OES) of nuclear masses, which were proven to be a helpful indicator on mirror energy differences in our previous studies [9,37]. The OES is defined as $2E_{\mathrm{OES}} = S_{2N} - 2S_N$. Here, S_N and S_{2N} are one-nucleon (either proton or neutron) and two-nucleon separation energies, respectively. The systematics of OES energies for even-A nitrogen isotopes and their mirror nuclei is presented in Fig. 6. Comparing the E_{OES} of proton-rich nuclei to that of their neutron-rich partners, the difference is small except for the mirror pair ^{20}Al–^{20}N. The corresponding value of E_{OES} difference related to the ^{20}Al–^{20}N pair is 0.76 MeV, which is remarkably large.

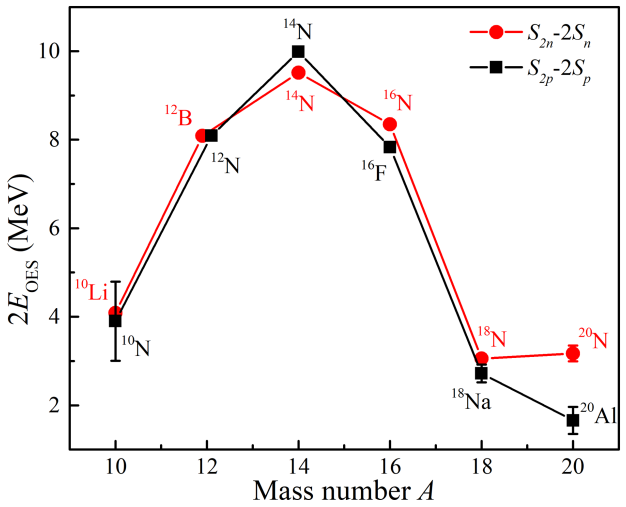

FIG. 6. The OES in nuclear masses for even-A nitrogen isotopes and their mirror nuclei. The solid circles represent the OES values calculated by the expression $2E_{\mathrm{OES}} = S_{2n} - 2S_n$, while the solid squares denote those calculated by the expression $2E_{\mathrm{OES}} = S_{2p} - 2S_p$. The data points for ^{12}B and ^{12}N are partially shifted in the x axis to avoid overlapping.

Appendix C: Estimation of half-life for ^{20}Al—We have estimated the half-life values for the observed ^{20}Al states by measuring distributions of their decay vertexes in the same way as in the previous study of $3p$ decay of ^{31}K [5]. All vertices are located within the reaction target, and therefore we found no indication on long-lived states in ^{20}Al. The width of the ^{20}Al g.s. derived by the description in Fig. 2 provides only the upper-limit value $\Gamma_{g.s.} < 400$ keV, which is mainly due to the experimental resolution. For comparison, the upper-limit Wigner estimate for a single-particle $1d_{3/2}$-shell width of the ^{20}Al g.s. is about 30 keV only.

Appendix D: Gamow shell model—The Gamow shell model utilizes the one-body Berggren basis [38], which includes bound, resonant, and scattering states. In GSM, many-body correlations are incorporated through configuration mixing, while continuum coupling is inherently accounted for at the basis level [23–25,39,40]. This allows GSM to effectively treat both continuum coupling and inter-nucleon correlations, making it a reliable predictive tool for describing weakly bound and unbound states, as demonstrated in Refs. [23,41,42]. GSM typically operates within a core-plus-valence-particle framework. In the present calculations, the interaction between the core and valence nucleons is modeled using a one-body Woods-Saxon (WS) potential, while the nucleon-nucleon interaction among

the valence nucleons is described by the effective field theory [43,44], as applied in previous studies, such as the four-proton decays in ^{18}Mg [42,45,46]. For the calculations of ^{20}Al, we adopt the doubly magic nucleus ^{14}O as the inner core, and use the Hamiltonian from Ref. [42], which was originally constructed for calculations involving ^{16}Ne and ^{18}Mg. Additionally, the leading-order $T = 0$ channels (V_s or V_t) are constrained to reproduce the ground state energy of ^{17}Ne. In the actual calculations, we first perform computations in the Berggren basis, where at most two nucleons (including valence protons and neutrons) are allowed to occupy scattering states, generating a natural orbital basis. Then, physical quantities are calculated within this natural orbital basis, where up to three protons or neutrons can occupy scattering states.

Appendix E: Gamow coupled-channel model—In the Gamow coupled-channel approach [26–28], ^{20}Al is considered as a system comprising a deformed core, ^{18}Mg, alongside a valence proton and neutron. Although this framework does not fully capture the unbound nature of this $3p$ emitter, we focus on the structural configuration of the valence nucleons. The relative motion between the valence nucleons and the core is described through Jacobi coordinates [26] with the Berggren ensemble [38]. To eliminate the Pauli-forbidden states, we apply a supersymmetric transformation [47,48]. For the interaction between the valence proton and neutron, we utilize the original Minnesota potential [49]. The core-valence nuclear potential adopts a WS form with the "universal" parameter set [50] and a quadrupole deformation $\beta_2 = -0.2$. To match the experimental spectrum of ^{19}Mg, we adjusted the depth of the WS central potential and the strength of its spin-orbit component to -43.9 MeV and 14.3 MeV, respectively. Additionally, we assume a dilatation-analytic form for the Coulomb potential between the core and the valence proton [51]. The calculations are performed within a model space constrained by $\max(l_x, l_y) \leq 7$, and the maximal hyperspherical quantum number $K_{\max} = 16$. To study resonances, the Berggren basis is applied to channels with $K \leq 3$, while for higher K channels, a harmonic oscillator basis with oscillator length $b = 1.75$ fm and $N_{\max} = 40$ is employed. The complex-momentum contour for the Berggren basis spans $k = 0 \rightarrow 0.3 - 0.02i \rightarrow 0.5 \rightarrow 1.2 \rightarrow 6$ fm^{-1}, being divided into 40 scattering states for each segment.